

This discussion paper is/has been under review for the journal Atmospheric Chemistry and Physics (ACP). Please refer to the corresponding final paper in ACP if available.

Effects of long-range aerosol transport on the microphysical properties of low-level liquid clouds in the Arctic

Q. Coopman^{1,2}, T. J. Garrett¹, J. Riedi², S. Eckhardt³, and A. Stohl³

¹Department of Atmospheric Sciences, University of Utah, Salt Lake City, UT, USA

²Laboratoire d'Optique Atmosphérique, Université de Lille/CNRS, France

³Norwegian Institute for Air Research, Keller, Norway

Received: 1 October 2015 – Accepted: 23 October 2015 – Published: 12 November 2015

Correspondence to: Q. Coopman (quentin.coopman@ed.univ-lille1.fr)

Published by Copernicus Publications on behalf of the European Geosciences Union.

ACPD

15, 31823–31866, 2015

Effects of pollution
on liquid clouds in
the Arctic

Q. Coopman et al.

Title Page

Abstract

Introduction

Conclusions

References

Tables

Figures

◀

▶

◀

▶

Back

Close

Full Screen / Esc

Printer-friendly Version

Interactive Discussion



Abstract

The properties of clouds in the Arctic can be altered by long-range aerosol transport to the region. The goal of this study is to use satellite, tracer transport model, and meteorological data sets to determine the effects of pollution on cloud microphysics due only to pollution itself and not to the meteorological state. Here, A-Train, POLDER-3 and MODIS satellite instruments are used to retrieve low-level liquid cloud microphysical properties over the Arctic between 2008 and 2010. Cloud retrievals are co-located with simulated pollution represented by carbon-monoxide concentrations from the FLEXPART tracer transport model. The sensitivity of clouds to pollution plumes – including aerosols – is constrained for cloud liquid water path, temperature, altitude, specific humidity, and lower tropospheric stability (LTS). We define an Indirect Effect (IE) parameter from the ratio of relative changes in cloud microphysical properties to relative variations in pollution concentrations. Retrievals indicate that, depending on the meteorological regime, IE parameters range between 0 and 0.34 for the cloud droplet effective radius, and between -0.10 and 0.35 for the optical depth, with average values of 0.12 ± 0.02 and 0.15 ± 0.02 respectively. The IE parameter increases with increasing specific humidity and LTS. Further, the results suggest that for a given set of meteorological conditions, the liquid water path of arctic clouds does not respond strongly to pollution. Or, not constraining sufficiently for meteorology may lead to artifacts that exaggerate the magnitude of the aerosol indirect effect. The converse is that the response of arctic clouds to pollution does depend on the meteorologic state. Finally, we find that IE values are highest when pollution concentrations are low, and that they depend on the source of pollution.

1 Introduction

Due to growing concentrations of green house gases, including atmospheric carbon dioxide (CO_2), the Arctic region has warmed approximately two times faster than the

Effects of pollution on liquid clouds in the Arctic

Q. Coopman et al.

[Title Page](#)

[Abstract](#)

[Introduction](#)

[Conclusions](#)

[References](#)

[Tables](#)

[Figures](#)

◀

▶

◀

▶

[Back](#)

[Close](#)

[Full Screen / Esc](#)

[Printer-friendly Version](#)

[Interactive Discussion](#)



global average due to feedback processes (Serreze and Francis, 2006; Serreze et al., 2009; Richter-Menge and Jeffries, 2011), a trend that is anticipated to continue through this century (Yoshimori et al., 2013; Overland and Wang, 2013). Further, the Arctic is not pristine, even if it is remote from industrialized areas and major aerosol sources.

5 Mid-latitude aerosols can be transported to northern latitudes in relatively high concentrations due to low precipitation and strong temperature inversions that inhibit vertical mixing (Sirois and Barrie, 1999; Law and Stohl, 2007; Quinn et al., 2007; Law et al., 2014). From spring to summer, the atmosphere becomes cleaner due to an increase in wet-scavenging (Garrett et al., 2010). The origins of arctic haze tend to be pollution 10 from Eurasia (Shaw, 1995; Stohl, 2006; Shindell et al., 2008; Aucellet et al., 2014), and boreal forest fires in North America, Eastern Europe and Siberia (Stohl, 2006; Stohl et al., 2007).

Such aerosols have the potential to alter cloud properties in the Arctic (Garrett and Zhao, 2006; Lance et al., 2011). On one hand, thin low-level clouds with more numerous 15 smaller droplets can radiate more long wave radiation thereby warming the surface (Garrett et al., 2002, 2004; Garrett and Zhao, 2006). On the other, polluted clouds can reflect more sunlight, leading to a cooling effect (Lubin and Vogelmann, 2007). Zhao and Garrett (2015) found that seasonal changes in surface radiation associated with haze pollution ranges from $+12.2 \text{ W m}^{-2}$ in February to -11.8 W m^{-2} in August. Annually averaged, the long-wave warming and shortwave cooling nearly compensate, 20 although the seasonal timing of the forcings may have implications for rates of sea ice melt (Belchansky et al., 2004; Markus et al., 2009).

The Influence of aerosols on cloud microphysical properties is often quantified using an Indirect Effect (IE) parameter, expressible as the ratio of relative changes in 25 cloud microphysical properties to variations in pollution concentrations, most typically aerosols (Feingold et al., 2001; Feingold; 2003b). Garrett et al. (2004) used ground-based measurements of the cloud droplet effective radius and dried aerosol light scattering at Barrow (Alaska) to retrieve an indirect effect value for the cloud droplet effective radius between 0.13 and 0.19. Satellite measurements show that IE values

Effects of pollution on liquid clouds in the Arctic

Q. Coopman et al.

[Title Page](#)

[Abstract](#)

[Introduction](#)

[Conclusions](#)

[References](#)

[Tables](#)

[Figures](#)

[◀](#)

[▶](#)

[◀](#)

[▶](#)

[Back](#)

[Close](#)

[Full Screen / Esc](#)

[Printer-friendly Version](#)

[Interactive Discussion](#)



for cloud droplet effective radius range from 0.02 to 0.20 for mid-latitude continental clouds (Nakajima et al., 2001; Feingold, 2003a; Lohmann and Feichter, 2005; Myhre et al., 2007) and from 0.03 to 0.15 for mid-latitude oceanic clouds (Bréon et al., 2002; Sekiguchi, 2003; Kaufman et al., 2005; Myhre et al., 2007; Costantino and Bréon, 2013; Wang et al., 2014). Satellite instruments have the advantage of providing data over large spatial scales, however satellite retrievals of aerosol concentrations are normally obtained from air columns close to the analyzed cloud. The assumption is made of a horizontally homogeneous plume both within and without the cloud (Nakajima et al., 2001; Feingold et al., 2001; Sekiguchi, 2003). For large-scale cloud studies, this method potentially introduces bias since it is not obvious that pollution should be uniform for different meteorological regimes.

Co-locating satellite cloud retrievals with passive pollution tracer output from a chemical transport model offers an alternative approach for assessing the effect of pollution on clouds. In this way, cloud microphysical properties and pollution concentrations can be estimated at the same time, location, and meteorological regime (Schwartz et al., 2002; Kawamoto et al., 2006; Avey et al., 2007). Active tracers experience both sources and sinks, for example through wet scavenging, dry deposition, and chemical reactions. Passive pollution tracers, on the other hand, are determined only by their source and subsequent dilution. Most importantly, passive tracers are decoupled from clouds and are unaffected by wet scavenging. What can be expressed is the orthogonal sensitivity of clouds to pollution in a manner that accounts for the possibility of aerosol removal. If aerosols are scavenged during long-range transport, for example, then the cloud sensitivity to pollution is low even if the sensitivity to aerosols remains high. An example of a passive tracer is carbon monoxide (CO), which is a combustion by-product and correlates with the anthropogenic Cloud Condensation Nuclei (CCN) close to pollution sources (Longley et al., 2005).

Most generally, the primary control on cloud microphysical properties is not aerosols but rather meteorological conditions during cloud formation (Chang and Coakley, 2007; Brenguier and Wood, 2009; Kim et al., 2008; Painemal et al., 2014; Andersen and Cer-

Effects of pollution on liquid clouds in the Arctic

Q. Coopman et al.

[Title Page](#)

[Abstract](#)

[Introduction](#)

[Conclusions](#)

[References](#)

[Tables](#)

[Figures](#)

◀

▶

◀

▶

[Back](#)

[Close](#)

[Full Screen / Esc](#)

[Printer-friendly Version](#)

[Interactive Discussion](#)



Title Page	
Abstract	Introduction
Conclusions	References
Tables	Figures
◀	▶
◀	▶
Back	Close
Full Screen / Esc	
Printer-friendly Version	
Interactive Discussion	



2 Data

The analyses in this study are based on a co-location of satellite retrievals of cloud properties, tracer transport model simulations of pollution locations and concentrations, and reanalysis data sets for meteorological fields.

5 2.1 Satellite cloud property retrievals

In this study we used two instruments, both part of the A-train mission (Stephens et al., 2002). The MODIS instrument on board the Aqua satellite measures 36 different spectral bands from 400 nm to 14 400 nm in wavelength. For retrievals of the effective radius, optical depth, and cloud top temperature we use Collection 5 Level-2 products (Platnick et al., 2003; King and Platnick, 2006). Cloud top temperature is derived from the 11 μm infrared band. Cloud droplet effective radius (r_e) and optical depth (τ) are retrieved from simultaneous cloud-reflectance measurements in three water absorbing bands (1.6, 2.1, 3.7 μm) and three non-absorbing bands (0.65, 0.86, 1.2 μm) (Platnick et al., 2003). The pixel resolution of the retrievals at nadir is 1 km for cloud microphysics and 5 km for cloud top temperature.

The POLDER-3 camera on the PARASOL satellite platform (Polarization & Anisotropy of Reflectances for Atmospheric Sciences coupled with Observations from a Lidar) captures a wide field of view through spectral, directional, and polarized measurements of reflected sunlight (Fougnie et al., 2007). Multidirectional observations allow for a pixel to be observed from up to sixteen different view angles. The instrument measures radiance in 9 spectral channels between 443 and 1020 nm, including three polarized channels at 490, 670 and 865 nm. POLDER-3 cloud microphysical properties retrievals have a 36 km^2 spatial resolution. Cloud top pressure is derived from the cloud oxygen pressure (Bréon and Colzy, 1999). Cloud top pressure retrieved by POLDER-3 appears to be a better proxy for low-level cloud height than MODIS cloud top pressure derived using a thermal signature assuming a given temperature profile (Buriez et al., 1997; Weisz et al., 2007; Tietze et al., 2011; Desmons et al., 2013).

Title Page	
Abstract	Introduction
Conclusions	References
Tables	Figures
◀	▶
◀	▶
Back	Close
Full Screen / Esc	
Printer-friendly Version	
Interactive Discussion	



**Effects of pollution
on liquid clouds in
the Arctic**

Q. Coopman et al.

[Title Page](#)[Abstract](#)[Introduction](#)[Conclusions](#)[References](#)[Tables](#)[Figures](#)[◀](#)[▶](#)[◀](#)[▶](#)[Back](#)[Close](#)[Full Screen / Esc](#)[Printer-friendly Version](#)[Interactive Discussion](#)

To determine the cloud thermodynamic phase we use a combination of MODIS and POLDER-3 measurements. The algorithm takes advantage of multi-angle polarization data, shortwave, thermal infrared, and visible measurements to retrieve a thermodynamic phase index Φ between 0 for liquid clouds and 200 for ice clouds with varying degrees of confidence (Riedi et al., 2010). Figure 1 shows the distribution of the thermodynamic phase index for clouds between 200 and 1000 m and between 1000 and 2000 m altitude from 2008 to 2010 over a region with latitudes greater than 65°. We observe different modes in the phase index corresponding to liquid clouds with Φ lower than 70, clouds with undetermined phase, mixed phase or multiple cloud layers, for which Φ lies between 70 and 140, and ice clouds with Φ greater than 140.

2.2 Anthropogenic pollution tracer fields

For determining anthropogenic pollution tracer fields, we used the Lagrangian particle dispersion model FLEXPART (Stohl et al., 1998, 2005). The model is driven with 3 hourly operational analysis wind fields from the European Centre for Medium-Range Weather Forecasts (ECMWF) with 91 model levels and a horizontal resolution of $1^\circ \times 1^\circ$. We used the same simulations as described by Stohl et al. (2013), which considered a black-carbon tracer undergoing removal processes, two fixed-lifetime black carbon tracers, and a carbon monoxide (CO) tracer. The CO tracer which has been used for this study was considered as passive in the atmosphere but was removed from the simulation 31 days after emission, thus focussing the simulation on “fresh” pollution. For the CO emission, ECLIPSE (Evaluating the CLimate and Air Quality ImPacts of Short-livED Pollutants) versions 4.0 emission data (Klimont et al., 2015; Stohl et al., 2015) were used. For the anthropogenic emissions considered here, the ECLIPSE emissions are based on the GAINS (Greenhouse gas – Air pollution Interactions and Synergies) model (Amann et al., 2011). The emissions were determined separately for every year of this study and, notably, include gas flaring emissions, which were shown to be important for black carbon in the Arctic (Stohl et al., 2013). Emissions from the

**Effects of pollution
on liquid clouds in
the Arctic**

Q. Coopman et al.

[Title Page](#)[Abstract](#)[Introduction](#)[Conclusions](#)[References](#)[Tables](#)[Figures](#)[|◀](#)[▶|](#)[◀](#)[▶](#)[Back](#)[Close](#)[Full Screen / Esc](#)[Printer-friendly Version](#)[Interactive Discussion](#)

residential sector were temporally disaggregated using a heating degree day approach (Stohl et al., 2013).

Studies that have used FLEXPART CO concentration fields (χ_{CO}) have found satisfactory agreement between model output and measurements (Stohl, 2006; Paris et al., 2009; Hirdman et al., 2010; Sodemann et al., 2011; Stohl et al., 2013, 2015; Eckhardt et al., 2015).

In the Alaskan Arctic on 18 April 2008, Warneke et al. (2009) described a slope of 0.9 for a linear fit between FLEXPART model output of χ_{CO} and airborne measurements of CO with a least-squares correlation coefficient of 0.63.

The FLEXPART model outputs used here have a temporal resolution of 3 h and a spatial resolution of $1^\circ \times 2^\circ$ (in latitude and longitude) divided into 9 different vertical levels. FLEXPART CO concentration (χ_{CO}) output is provided in units of mg m^{-3} but converted to units of ppbv (parts per billion by volume) to remove the atmospheric pressure dependence. Since the focus here is on the effect of anthropogenic pollution on clouds, only FLEXPART spatial bins where anthropogenic sources comprise more than 80 % of total CO concentrations are considered for comparison with cloud properties.

2.3 Meteorological data

ERA-Interim (ERA-I) reanalysis data from ECMWF (Berrisford et al., 2009) extends from 1989 to the present with an improved version released in 2011 (Dee et al., 2011).

The temporal resolution is 6 h at 60 pressure levels. Reanalysis data from ERA-I shows good agreement with satellite retrievals and aircraft data for cloud fraction and cloud radiative forcing in the Arctic (Zygmuntowska et al., 2012). Wesslén et al. (2014) analyzed ERA-I data with the Arctic Cloud-Ocean Study (ASCOS) campaign measurements in 2008 and calculated biases of about 1.3°C , 1 % and -1.5 hPa respectively for temperature, relative humidity and surface pressure, root mean square errors of about 1.9°C , 3.7 % and 8.7 hPa respectively, and correlation coefficients of approximately 0.85 for temperature and surface pressure and 0.31 for the relative humidity.

Title Page	
Abstract	Introduction
Conclusions	References
Tables	Figures
◀	▶
◀	▶
Back	Close
Full Screen / Esc	
Printer-friendly Version	
Interactive Discussion	

The goal of this study is to use satellite, tracer transport model, and meteorological data sets to determine the effects of pollution on cloud microphysics due only to pollution itself and not to the meteorological state. The focus is on temperature, specific humidity, and LTS since these have been identified as a basic meteorological quantities that correlate with cloud microphysical properties (Matsui et al., 2006; Mauger and Norris, 2007). Defining the potential temperature (θ) as

$$\theta = T \cdot \left(\frac{P_0}{P} \right)^{\frac{R}{c_p}} \quad (1)$$

where T and P are the air temperature and pressure, P_0 equals 1000 hPa and R , and c_p are respectively the gas constant for air, and the isobaric heat capacity, the LTS is defined as the potential temperature difference between 700 and 1000 hPa (Klein and Hartmann, 1993).

$$\text{LTS} = \theta_{700} - \theta_{1000} \quad (2)$$

We also consider clouds with values of LWP greater than 40 g m^{-2} separately from clouds with LWP values less than 40 g m^{-2} . This approach separates clouds according to their thermal radiative properties since a cloud with low LWP will tend to act as a graybody and potentially be more radiatively susceptible to pollution in the thermal infrared (Garrett and Zhao, 2006; Lubin and Vogelmann, 2006; Mauritsen et al., 2011). Thick clouds act as blackbodies, and their longwave radiative properties are determined by temperature only (Garrett and Zhao, 2006; Garrett et al., 2009).

The different data sets used in this article are summarized in Table 1.

3 Methodology

This study examines data between 2008 and 2010 over the ocean at latitudes greater than 65° . Passive satellites sensors need sunlight to retrieve clouds microphysical pa-



rameters of interest from visible wavelength measurements so analyses are restricted to the period between 1 March and 30 September.

3.1 Co-location of satellite retrieval and model pollution tracer fields

CO tracer concentrations from a FLEXPART grid cell are defined as the average between two temporal points, averaged over a spatial box. For example, model CO concentrations at 03:00 UTC and at the latitude–longitude co-ordinates of (70°, 80°), represent an average over a box between the latitudes of 70 to 71° and longitudes of 80 to 82° and between 00:00 UTC and 03:00 UTC.

For an A-train satellite overpass time of 00:45 UTC, we match space-based retrievals to FLEXPART concentration output at 03:00 UTC representing the average concentration between 00:00 UTC to 03:00 UTC and then linearly interpolate ECMWF meteorological fields to the LTS and specific humidity values for 01:30 UTC.

Here, as with many prior studies looking at aerosol–cloud interactions in the Arctic, we consider only low-level clouds (Garrett et al., 2004; Garrett and Zhao, 2006; Lubin and Vogelmann, 2006; Mauritsen et al., 2011), in layers between 200 and 1000 m, and between 1000 and 2000 m. These two layers correspond to the FLEXPART vertical bin resolution. We average POLDER and MODIS data that falls within the height bins so they are co-located with the corresponding FLEXPART CO concentrations.

Regarding horizontal co-location, Fig. 2 represents how the datasets are combined. We project data from satellite, model, and reanalysis data sets onto an equal-area sinusoidal grid such that the grid-cell resolution is $0.5^\circ \times 0.5^\circ$ at the equator corresponding to an area of $54\text{ km} \times 54\text{ km}$. The sinusoidal projection conserves the grid-cell area independently of longitude and latitude. One grid-cell can include up to 81 POLDER-MODIS pixels. Satellite and tracer transport model data are averaged over each grid-cell.

One consequence of the averaging is that each grid-cell can include up to 81 different pixel-level values of Φ . We place a limit on the SD of the averaged phase index within each grid-cell such that $\sigma_\Phi < 10$ in order to satisfy an a priori requirement of there being a nearly homogeneous phase within each grid cell.

[Title Page](#)

[Abstract](#)

[Introduction](#)

[Conclusions](#)

[References](#)

[Tables](#)

[Figures](#)

◀

▶

◀

▶

[Back](#)

[Close](#)

[Full Screen / Esc](#)

[Printer-friendly Version](#)

[Interactive Discussion](#)



3.2 The indirect effect parameter

Assuming a constant LWC and a mono-disperse size distribution of cloud droplets, the droplet effective radius (r_e) decreases as the droplet number concentration N_c increases following the relation (Feingold et al., 2001):

$$5 \quad \frac{\partial \ln r_e}{\partial \ln N_c} \Big|_{LWP} = -\frac{1}{3} \quad (3)$$

Here, we take a different approach which is to examine the sensitivity of clouds properties to the CO tracer under the presumption that the CO tracer serves as a proxy for the potential of pollution, of which CCN may be a part, to modify N_c . Of course, N_c and CO tracer concentrations (χ_{CO}) do not represent the same quantity. However, cloud condensation nuclei and CO are both by-products of combustion. The two quantities are expected to be highly correlated close to pollution sources (Avey et al., 2007; Tietze et al., 2011). Thus, the indirect effect parameter could be expressed alternatively as:

$$IE_\tau = \frac{d \ln \tau}{d \ln \chi_{CO}} \quad (4)$$

$$15 \quad IE_{r_e} = -\frac{d \ln r_e}{d \ln \chi_{CO}} \quad (5)$$

For example, if N_c , from Eq. (3) is linearly related with χ_{CO} then Eq. (5) has as its theoretical maximum value of $IE_{r_e} = 1/3$.

Further from source regions, the correlation of CO concentration and aerosols is invariant to dilution but it is sensitive to wet and dry scavenging (Garrett et al., 2010, 2011). When aerosol scavenging rates are low, CO and CCN will tend to covary. Values of IE tend to be lower when precipitation is high along transport pathways and aerosols are removed. Garrett et al. (2010) found that at Barrow, Alaska, when the temperature

[Title Page](#)

[Abstract](#)

[Introduction](#)

[Conclusions](#)

[References](#)

[Tables](#)

[Figures](#)

◀

▶

◀

▶

[Back](#)

[Close](#)

[Full Screen / Esc](#)

[Printer-friendly Version](#)

[Interactive Discussion](#)



Effects of pollution on liquid clouds in the Arctic

Q. Coopman et al.

Title Page	
Abstract	Introduction
Conclusions	References
Tables	Figures
◀	▶
◀	▶
Back	Close
Full Screen / Esc	
Printer-friendly Version	
Interactive Discussion	

exceeds 4 °C at the surface, wet scavenging efficiently removes CCN from the atmosphere and cloud microphysical properties are not affected by pollution even if the CO remains. Moreover, the simulated CO tracer by the transport model FLEXPART can be de-correlated from the real pollution loading, which can introduce scatter in the results presented here. Effectively, what is expressed by Eq. (4) and (5) is not the sensitivity of clouds to aerosols, but rather their sensitivity to pollution, taking into account the possibility that the cloud active component of the polluted air parcel may have been removed. The analysis becomes less focussed on the local physics and more focussed on the actual impact of anthropogenic activities on clouds far from the combustion source.

Since r_e and the optical depth (τ) are linked through $\tau = \frac{3}{2} \frac{LWP}{\rho_w r_e}$ it follows that

$$\frac{\partial \ln \tau}{\partial \ln \chi_{CO}} = -\frac{\partial \ln r_e}{\partial \ln \chi_{CO}} + \frac{\partial \ln LWP}{\partial \ln \chi_{CO}} \quad (6)$$

or,

$$IE_\tau = IE_{r_e} + IE_{LWP} \quad (7)$$

Figure 3 shows an IE retrieval example for temperatures between –12 and 6 °C and altitudes between 1000 and 2000 m, for all LWP values. We first calculate IE_{r_e} as the linear fit of the natural logarithm of the effective radius to the natural logarithm of CO concentrations. The fit used in this study is based on the robust linear method (RLM) (Huber, 1973, 1981; Venables and Ripley, 2013). RLM uses an iterative least squares algorithm: every measurement has initially the same weight; The weights of each point are updated giving a lower weight to points which appear as outliers with respect to the entire dataset. The process iterates several times and stops when the convergence tolerance of the estimated fitting coefficients are below 10^{-8} . The slope is therefore less sensitive to outlier points. In the example of Fig. 3, the slope retrieved by the linear fit is -0.13 ± 0.016 . Referring to Eq. (5), IE_{r_e} equals to $+0.13 \pm 0.016$.



3.3 Constraining IE for specific humidity and lower tropospheric stability

Figure 4 presents a 2-D histogram of frequency distribution of the specific humidity and the LTS. The LTS ranges from 2.1 to 37 K and the specific humidity from 0.13 to 11 g kg⁻¹. The median values for specific humidity and LTS are 2.0 g kg⁻¹ and 19 K respectively.

Table 2 describes the method used here for constraining values of IE for meteorological conditions. We identify a range in LTS and specific humidity that occupies 15% of the total space of observed values but that is centered at the mode of the respective distributions. The total LTS range is 2.1 to 37 K, so the interval size is 5.3 K. Specific humidity is more logarithmically distributed. The logarithm base 10 of specific humidity has an interval of 0.28. The most common values of meteorological state, defined here as the maximum number of measurements, are delimited by the red rectangle in Fig. 4 corresponding to a range between 0.30 and 0.60 for the logarithm of specific humidity, corresponding to a range of 2.0 g kg⁻¹ to 4.0 g kg⁻¹, and a range of 16.5 K to 21.8 K for LTS. It is these ranges that are focussed upon for calculation of the IE parameter. We assume these intervals are sufficiently narrow that the variability within the interval has limited impact on the cloud microphysics.

4 Results

4.1 The indirect effect

Figure 5 summarizes IE values calculated using combined POLDER-3, MODIS, and FLEXPART data for the period between 2008 and 2010 for latitudes greater than 65° over ocean, and constrained for cloud top temperature in bins of 2° between -12 and 6 °C. The results are categorized according to bins in temperature, altitude and LWP, and are constrained for LTS and specific humidity. The number of grid-cells used to calculate each IE parameter per bin ranges from 100 to 3300. The IE parameter is

Title Page	
Abstract	Introduction
Conclusions	References
Tables	Figures
◀	▶
◀	▶
Back	Close
Full Screen / Esc	
Printer-friendly Version	
Interactive Discussion	



[Title Page](#)[Abstract](#)[Introduction](#)[Conclusions](#)[References](#)[Tables](#)[Figures](#)[|](#)[|](#)[◀](#)[▶](#)[Back](#)[Close](#)[Full Screen / Esc](#)[Printer-friendly Version](#)[Interactive Discussion](#)

almost always positive but sometimes close to zero. IE_{r_e} ranges from 0 for graybody clouds between 1000 to 2000 m altitude with a cloud top temperature between -6 and -4 °C, to 0.34 for blackbody clouds between 1000 and 2000 m altitude with a cloud top temperature between 4 and 6 °C. IE_τ ranges from -0.10 for all clouds between 200 to 1000 m altitude with a cloud top temperature of -11 °C, to 0.35 at 3 °C for blackbody clouds between 1000 and 2000 m altitude. In general, IE_τ and IE_{r_e} are of the same order of magnitude and the maximum values of IE are found for clouds with temperatures above the freezing temperature.

We define the uncertainty in IE as the 95 % confidence limit in the calculation of the slope of the linear fit. The uncertainty in the calculated values of IE_{r_e} is generally less than 0.1, except for clouds with temperatures between 4 and 6 °C and between -12 and -10 °C where the uncertainty bar is approximately 0.2. For the optical depth, the uncertainty is typically approximately 0.1, although larger values are observed for high and low cloud top temperatures.

For blackbody clouds between 1000 and 2000 m altitude, the average values of IE_τ and IE_{r_e} equal 0.20 and 0.14 respectively. For cloud tops between 200 and 1000 m altitude, IE_τ and IE_{r_e} equal 0.14. For graybody clouds between 1000 and 2000 m, IE_τ and IE_{r_e} equal 0.12 and 0.08 respectively. For cloud tops between 200 and 1000 m altitude, IE_τ and IE_{r_e} equals 0.14 and 0.12 respectively. The value of IE appears to be fairly robust to altitude and cloud thickness and to whether r_e or τ is considered. Table 3 presents the average IE_τ and IE_{r_e} . In all case cases, values are near 0.13 ± 0.03 .

4.2 Dependence of IE on pollution concentration, specific humidity, and lower tropospheric stability

Table 4 shows values of IE_{r_e} and IE_τ for graybody and blackbody clouds, and for $\chi_{CO} < 5.5$ ppbv and $\chi_{CO} > 10.0$ ppbv, corresponding respectively to the lower and upper quartile of CO tracer concentration, and constrained for LTS and specific humidity. For graybody and blackbody clouds, IE_τ and IE_{r_e} are highest for low values of χ_{CO} . The difference in IE values between low and high polluted environments is slightly greater

for IE_{r_e} than IE_τ . Table 4 suggests that cloud effective radius and cloud optical depth are most sensitive to pollution when pollution concentrations are low. Previous studies have hypothesized that the effect of CCN on cloud microphysical properties saturates when cloud droplet concentrations are high (Bréon et al., 2002; Andersen and Cermak, 2015). This effect does not explain the differences presented in Table 4 because Eq. (4) and (5) already take into account the potential for linear saturation by considering the logarithmic values of χ_{CO} and cloud parameters.

We now present the sensitivity of the IE parameter to different regimes of meteorological parameters define by bins delimited by the percentiles presented in Table 5. For each parameter we define 5 different regimes – from the bin minimum to 20th percentile to the bin 80th percentile to maximum. Figures 6 and 7 show the influence of pollution loading on the cloud droplet effective radius and cloud optical depth for each of the different specific humidity and LTS regimes. Figure 6 presents the IE parameter with respect to the cloud optical depth and cloud droplet effective radius as a function of the specific humidity, constraining for LTS according to the method described in Sect. 3.3. Figure 7 is the same as Fig. 6 except that it shows IE as a function of LTS for a range of specific humidities.

Figure 6 shows that IE_{r_e} and IE_τ tend to increase with the specific humidity independent of LTS. The IE parameter is close to zero, or negative, for low values of specific humidity. It increases rapidly with specific humidity, saturating at a maximum value of about 2.5 g kg^{-1} . We note that cloud top temperature and specific humidity are weakly correlated. The correlation coefficient (r^2) of the linear regression of the two parameters is 0.20.

IE_{r_e} increases with LTS, from 0.02 for values of LTS ranging between 2.1 and 14 K, to 0.09 for values of LTS between 23 and 38 K. The IE_τ dependance on LTS is larger: IE_τ equals 0.10 for LTS values between 2.1 and 14 K and it equals 0.32 for LTS values between 21 and 38 K.

[Title Page](#)[Abstract](#)[Introduction](#)[Conclusions](#)[References](#)[Tables](#)[Figures](#)[◀](#)[▶](#)[◀](#)[▶](#)[Back](#)[Close](#)[Full Screen / Esc](#)[Printer-friendly Version](#)[Interactive Discussion](#)

5 Discussion

The results presented here show values of the IE parameter with respect to the cloud droplet effective radius and optical depth, for clouds over oceans north of 65° lying between 200 and 2000 m, and for the years between 2008 to 2010. We find IE values which range from 0.0 to 0.34 for the cloud droplet effective radius, and from -0.1 to 0.35 for the optical depth.

Prior studies examining the Arctic region have retrieved IE values ranging from -0.10 to 0.40 (Garrett et al., 2004; Lihavainen et al., 2009; Zhao et al., 2012, Sporre et al., 2012). Tietze et al. (2011) calculated IE values ranging from 0.0 to 0.17 using a similar satellite-FLEXPART co-location method presented here. What differs is that we are examining solely anthropogenic pollution, we extend the dataset from one to three years, and we constrain for specific humidity and LTS. The larger IE values we find in this study suggest a higher sensitivity of cloud microphysical properties to pollution than was found by Tietze et al. (2011).

However, Tietze et al. (2011) also found values of IE_{τ} that were greater than IE_{r_e} , by a factor of up to four, and they attributed this difference to unknown dynamic or precipitation feedbacks that make IE_{LWP} greater than zero (Eq. 7). In contrast, our results show that the IE_{r_e} and IE_{τ} parameters are more similar, suggesting no such feedback. Table 6 compares the differences between IE_{τ} and IE_{r_e} that are presented in Table 3, along with their corresponding values when the data are not constrained for specific humidity and LTS. The difference between IE_{r_e} and IE_{τ} is largest when the data are not constrained for meteorological parameters. For all clouds considered, the maximum difference increases from 0.04 when the data are constrained to 0.12 when the data are not constrained. This is important since it suggests that the hypothesized feedbacks discussed by Tietze et al. (2011) may have in fact been due to the natural sensitivity of clouds to local meteorology. Not constraining sufficiently for meteorology may lead to artifacts that exaggerate the magnitude of the aerosol indirect effect.

[Title Page](#)[Abstract](#)[Introduction](#)[Conclusions](#)[References](#)[Tables](#)[Figures](#)[◀](#)[▶](#)[◀](#)[▶](#)[Back](#)[Close](#)[Full Screen / Esc](#)[Printer-friendly Version](#)[Interactive Discussion](#)

In contrast to most prior efforts, satellite-retrieved cloud properties are not compared to CCN or aerosol concentrations but rather to pollution concentrations – specifically CO simulated from a tracer transport model. For temperatures below -6°C , low values of IE are observed. Tietze et al. (2011) hypothesized that at such temperatures, cloud supersaturations may be too small to activate aerosols as CCN or that clouds with colder temperatures have followed longer transport pathways nearer the surface (Stohl, 2006) and therefore had greater exposure to dry deposition.

Table 4 suggests that IE values are lowest when pollution concentration is high. Figure 8 presents the normalized distribution of potential temperature for polluted and pristine clouds, defined as the upper and lower quartile, for graybody clouds. We present results for graybody clouds because the IE differences between polluted and clean cases are largest; Results for blackbody and all clouds are not shown here, but have similar results regarding the potential temperature distribution.

Highly polluted air parcels are associated with potential temperatures around 280 K whereas pristine air parcels have a lower potential temperature – around 272 K. We hypothesize that higher values of potential temperature suggest pollution sources from further south, so wet scavenging is more likely to occur during transport and this decreases the correlation between CO tracer and CCN, therefore lowering the IE parameter. Also, polluted air parcel and aerosols do not necessarily have the same physical and chemical properties at lower and higher latitudes, and this difference may impact the influence of aerosols on cloud microphysics and aerosols (Bilde and Svenningsson, 2004; Dusek et al., 2006; Ervens et al., 2007; Andreae and Rosenfeld, 2008).

In general, we observe that when the moisture increases, the cloud sensitivity to pollution increases. From model simulations based of stratocumulus Ackerman et al. (2004) found that when the relative humidity (RH) above cloud top is high, cloud LWP increases with N_c consistent with theoretical arguments (Albrecht, 1989; Pincus and Baker, 1994), but that when the RH is low, the LWP decreases when N_c increases, as supported by some observations (Coakley and Walsh, 2002). The difference was attributed to the consequence of dry air into a cloud layer. Humidity inversions are

[Title Page](#)[Abstract](#)[Introduction](#)[Conclusions](#)[References](#)[Tables](#)[Figures](#)[◀](#)[▶](#)[◀](#)[▶](#)[Back](#)[Close](#)[Full Screen / Esc](#)[Printer-friendly Version](#)[Interactive Discussion](#)

Effects of pollution on liquid clouds in the Arctic

Q. Coopman et al.

[Title Page](#)

[Abstract](#)

[Introduction](#)

[Conclusions](#)

[References](#)

[Tables](#)

[Figures](#)

◀

▶

◀

▶

[Back](#)

[Close](#)

[Full Screen / Esc](#)

[Printer-friendly Version](#)

[Interactive Discussion](#)



common above low-level cloud tops in the Arctic (Nygård et al., 2014), so similar phenomena may be playing a role.

Studies of the indirect effect at mid-latitudes suggest that values of IE are highest under unstable conditions (Chen et al., 2014; Andersen and Cermak, 2015). Our results show that in the Arctic, the impact of LTS on IE is the reverse. Klein and Hartmann (1993) showed that, in general, higher values of LTS lead to greater stratiform cloudiness, except in the Arctic where radiative cooling prevails over convection as the driving mechanism for cloud formation.

Finally, we find IE_{τ} is more sensitive to changes in LTS than IE_{r_e} . A consequence is that for values of LTS greater than the eightieth percentile bin of 23 K, IE_{τ} and IE_{r_e} differ by about 0.20. In a stable atmosphere with high LTS it appears that IE_{LWP} increases more strongly in response to aerosols than in unstable environments (Klein and Hartmann, 1993; Qiu et al., 2015).

6 Conclusions

Satellite, numerical model, and meteorological reanalyses data sets from 2008 to 2010 have been used here to calculate the sensitivity of cloud droplet effective radius and optical depth in the Arctic to anthropogenic polluted air parcels transported from mid-latitudes. We focussed on latitudes north of 65° for the period between March 2008 and October 2010. Using ECMWF reanalysis data, we constrained the sensitivity analysis for temperature, LTS, specific humidity, altitude, and LWP. We find values of IE close to the theoretical maximum of 1/3, assuming that a simulated CO tracer correlates well with CCN. IE_{r_e} and IE_{τ} seem to increase with specific humidity and LTS, highlighting that meteorological parameters have an important impact on aerosols influence with cloud microphysical properties.

Globally, Klimont et al. (2013) have estimated that there was a drop of about 9281 Gg in anthropogenic sulphur dioxide emissions between 2005 and 2010 due to a reduction in European and American emissions and a flue gas desulfurization program on

power plants in China. This reduction in emissions has lead to a decrease of sulfate concentrations at Arctic surface station (Hirdman et al., 2010). In the Arctic, the effect of a decrease in mid-latitude pollution emissions may be some day offset by greater levels of Arctic industrialization (Lindholt and Glomsrød, 2012) and shipping (Pizzolato et al., 2014; Miller and Ruiz, 2014) that introduce new local aerosol sources. Further, an increase in the extent of open-ocean due to sea-ice retreat may be expected to lead to an increase in the atmospheric humidity (Boisvert and Stroeve, 2015) and from the results presented here, a higher sensitivity of clouds to aerosols. However, this study also suggests that any associated decrease in LTS may be expected to counter-act this effect. Sea-ice retreat would also enhance dimethyl sulfide emissions, potentially increasing cloud cover in the Arctic (Ji et al., 2013).

Climate warming is thought to stimulate boreal forest fires (Westerling et al., 2006). The impact of pollution from biomass burning has not been included in the present research. Given biomass burning aerosol can act as efficient ice nuclei (Markus et al., 2009), the analyses presented here might be extended to explore aerosol-induced changes in cloud thermodynamic phase.

Acknowledgements. This paper is dedicated posthumously to Kyle Tietze, who developed many of the techniques used in this study while a graduate student at the University of Utah. The authors thank ICARE, NASA and CNES for the data used in this research. We acknowledge financial support from The University of Lille1. This material is based upon work supported by the National Science Foundation under the Grant No. 1303965. NILU researchers have received funding from the European Union Seventh Framework Programme (FP7/2007-2013) under grant agreement no. 282688 – ECLIPSE.

References

- Ackerman, A. S., Kirkpatrick, M. P., Stevens, D. E., and Toon, O. B.: The impact of humidity above stratiform clouds on indirect aerosol climate forcing, *Nature*, 432, 1014–1017, doi:10.1038/nature03137.1, 2004. 31839

Effects of pollution on liquid clouds in the Arctic

Q. Coopman et al.

[Title Page](#)

[Abstract](#)

[Introduction](#)

[Conclusions](#)

[References](#)

[Tables](#)

[Figures](#)

◀

▶

◀

▶

[Back](#)

[Close](#)

[Full Screen / Esc](#)

[Printer-friendly Version](#)

[Interactive Discussion](#)



Effects of pollution on liquid clouds in the Arctic

Q. Coopman et al.

[Title Page](#)

[Abstract](#)

[Introduction](#)

[Conclusions](#)

[References](#)

[Tables](#)

[Figures](#)

◀

▶

[Back](#)

[Close](#)

[Full Screen / Esc](#)

[Printer-friendly Version](#)

[Interactive Discussion](#)



- Brenguier, J. and Wood, R.: Observational strategies from the micro to meso scale, in: Clouds in the Perturbed Climate System: Their Relationship to Energy Balance, Atmospheric Dynamics, and Precipitation, edited by: Heintzenberg, J. and Charlson, R. J., 487–510, available at: ftp://ftp-projects.zmaw.de/aerocom/meetings/frankfurt_2007/brenguier.pdf (last access: 11 November 2015), MIT Press, MASS, Cambridge, 2009. 31826
- Bréon, F.-M. and Colzy, S.: Cloud detection from the spaceborne POLDER instrument and validation against surface synoptic observations, *J. Appl. Meteorol.*, 38, 777–785, doi:10.1175/1520-0450(1999)038<0777:CDFTSP>2.0.CO;2, 1999. 31828
- Bréon, F.-M., Tanré, D., and Generoso, S.: Aerosol effect on cloud droplet size monitored from satellite, *Science* (New York, N. Y.), 295, 834–8, doi:10.1126/science.1066434, 2002. 31826, 31837
- Buriez, J. C., Vanbause, C., Parol, F., Goloub, P., Herman, M., Bonnel, B., Fouquart, Y., Couvert, P., and Seze, G.: Cloud detection and derivation of cloud properties from POLDER, *Int. J. Remote Sens.*, 18, 2785–2813, doi:10.1080/014311697217332, 1997. 31828
- Chang, F. L. and Coakley, J. A.: Relationships between marine stratus cloud optical depth and temperature: Inferences from AVHRR observations, *J. Climate*, 20, 2022–2036, doi:10.1175/JCLI4115.1, 2007. 31826
- Chen, Y.-C., Christensen, M. W., Stephens, G. L., and Seinfeld, J. H.: Satellite-based estimate of global aerosol–cloud radiative forcing by marine warm clouds, *Nat. Geosci.*, advance on, 7, 643–646, doi:10.1038/ngeo2214, 2014. 31827, 31840
- Coakley, J. A. and Walsh, C. D.: Limits to the aerosol indirect radiative effect derived from observations of ship tracks, *J. Atmos. Sci.*, 59, 668–680, doi:10.1175/1520-0469(2002)059<0668:LTTAIR>2.0.CO;2, 2002. 31839
- Costantino, L. and Bréon, F. M.: Aerosol indirect effect on warm clouds over South-East Atlantic, from co-located MODIS and CALIPSO observations, *Atmos. Chem. Phys.*, 13, 69–88, doi:10.5194/acp-13-69-2013, 2013. 31826
- Dee, D. P., Uppala, S. M., Simmons, A. J., Berrisford, P., Poli, P., Kobayashi, S., Andrae, U., Balmaseda, M. A., Balsamo, G., Bauer, P., Bechtold, P., Beljaars, A. C. M., van de Berg, L., Bidlot, J., Bormann, N., Delsol, C., Dragani, R., Fuentes, M., Geer, A. J., Haimberger, L., Healy, S. B., Hersbach, H., Hölm, E. V., Isaksen, L., Källberg, P., Köhler, M., Matricardi, M., McNally, A. P., Monge-Sanz, B. M., Morcrette, J. J., Park, B. K., Peubey, C., de Rosnay, P., Tavolato, C., Thépaut, J. N., and Vitart, F.: The ERA-Interim reanalysis: Configuration and

Title Page	
Abstract	Introduction
Conclusions	References
Tables	Figures
◀	▶
◀	▶
Back	Close
Full Screen / Esc	
Printer-friendly Version	
Interactive Discussion	



performance of the data assimilation system, *Q. J. Roy. Meteorol. Soc.*, 137, 553–597, doi:10.1002/qj.828, 2011. 31830

Desmots, M., Ferlay, N., Parol, F., McHarek, L., and Vanbauce, C.: Improved information about the vertical location and extent of monolayer clouds from POLDER3 measurements in the oxygen A-band, *Atmos. Meas. Tech.*, 6, 2221–2238, doi:10.5194/amt-6-2221-2013, 2013. 31828

Dusek, U., Frank, G. P., Hildebrandt, L., Curtius, J., Schneider, J., Walter, S., Chand, D., Drewnick, F., Hings, S., Jung, D., Borrmann, S., and Andreae, M. O.: Size matters more than chemistry for cloud-nucleating ability of aerosol particles, *Science (New York, N. Y.)*, 312, 1375–1378, doi:10.1126/science.1125261, 2006. 31839

Eckhardt, S., Quennehen, B., Olivie, D. J. L., Berntsen, T. K., Cherian, R., Christensen, J. H., Collins, W., Crepinsek, S., Daskalakis, N., Flanner, M., Herber, A., Heyes, C., Hodnebrog, Ø., Huang, L., Kanakidou, M., Klimont, Z., Langner, J., Law, K. S., Lund, M. T., Mahmood, R., Massling, A., Myriokefalitakis, S., Nielsen, I. E., Nørgaard, J. K., Quaas, J., Quinn, P. K., Raut, J.-C., Rumbold, S. T., Schulz, M., Sharma, S., Skeie, R. B., Skov, H., Uttal, T., von Salzen, K., and Stohl, A.: Current model capabilities for simulating black carbon and sulfate concentrations in the Arctic atmosphere: a multi-model evaluation using a comprehensive measurement data set, *Atmos. Chem. Phys.*, 15, 9413–9433, doi:10.5194/acp-15-9413-2015, 2015. 31830

Ervens, B., Cubison, M., Andrews, E., Feingold, G., Ogren, J. A., Jimenez, J. L., DeCarlo, P., and Nenes, A.: Prediction of cloud condensation nucleus number concentration using measurements of aerosol size distributions and composition and light scattering enhancement due to humidity, *J. Geophys. Res.-Atmos.*, 112, 1–15, doi:10.1029/2006JD007426, 2007. 31839

Feingold, G.: Modeling of the first indirect effect: Analysis of measurement requirements, *Geophys. Res. Lett.*, 30, 30, 1997, doi:10.1029/2003GL017967, 2003a. 31826

Feingold, G.: First measurements of the Twomey indirect effect using ground-based remote sensors, *Geophys. Res. Lett.*, 30, 19–22, doi:10.1029/2002GL016633, 2003b. 31825

Feingold, G., Remer, L. A., Ramaprasad, J., and Kaufman, Y. J.: Analysis of smoke impact on clouds in Brazilian biomass burning regions: An extension of Twomey's approach, *J. Geophys. Res.*, 106, 22907–22922, 2001. 31825, 31826, 31833

Effects of pollution on liquid clouds in the Arctic

Q. Coopman et al.

[Title Page](#)

[Abstract](#)

[Introduction](#)

[Conclusions](#)

[References](#)

[Tables](#)

[Figures](#)

◀

▶

◀

▶

[Back](#)

[Close](#)

[Full Screen / Esc](#)

[Printer-friendly Version](#)

[Interactive Discussion](#)



Effects of pollution on liquid clouds in the Arctic

Q. Coopman et al.

[Title Page](#)

[Abstract](#)

[Introduction](#)

[Conclusions](#)

[References](#)

[Tables](#)

[Figures](#)

◀

▶

◀

▶

[Back](#)

[Close](#)

[Full Screen / Esc](#)

[Printer-friendly Version](#)

[Interactive Discussion](#)



Fougnie, B., Bracco, G., Lafrance, B., Ruffel, C., Hagolle, O., and Tiné, C.: PARASOL in-flight calibration and performance, *Appl. Optics*, 46, 5435–5451, doi:10.1364/AO.46.005435, 2007. 31828

Garrett, T. J. and Zhao, C.: Increased Arctic cloud longwave emissivity associated with pollution from mid-latitudes, *Letters*, 440, 787–789, doi:10.1038/nature04636, 2006. 31825, 31831, 31832

Garrett, T. J., Radke, L. F., and Hobbs, P. V.: Aerosol Effects on Cloud Emissivity and Surface Longwave Heating in the Arctic, *J. Atmos. Sci.*, 59, 769–778, doi:10.1175/1520-0469(2002)059<0769:AEOCEA>2.0.CO;2, 2002. 31825

10 Garrett, T. J., Zhao, C., Dong, X., Mace, G. G., and Hobbs, P. V.: Effects of varying aerosol regimes on low-level Arctic stratus, *Geophys. Res. Lett.*, 31, L17105, doi:10.1029/2004GL019928, 2004. 31825, 31832, 31838

15 Garrett, T. J., Maestras, M. M., Krueger, S. K., and Shmidt, C. T.: Acceleration by aerosol of a radiative-thermodynamic cloud feedback influencing Arctic surface warming, *Geophys. Res. Lett.*, 36, L19804, doi:10.1029/2009GL040195, 2009. 31831

Garrett, T. J., Zhao, C., and Novelli, P. C.: Assessing the relative contributions of transport efficiency and scavenging to seasonal variability in Arctic aerosol, *Tellus B*, 62, 190–196, doi:10.1111/j.1600-0889.2010.00453.x, 2010. 31825, 31833

20 Garrett, T. J., Brattström, S., Sharma, S., Worthy, D. E. J., and Novelli, P.: The role of scavenging in the seasonal transport of black carbon and sulfate to the Arctic, *Geophys. Res. Lett.*, 38, L16805, doi:10.1029/2011GL048221, 2011. 31833

Hirdman, D., Sodemann, H., Eckhardt, S., Burkhardt, J. F., Jefferson, A., Mefford, T., Quinn, P. K., Sharma, S., Ström, J., and Stohl, A.: Source identification of short-lived air pollutants in the Arctic using statistical analysis of measurement data and particle dispersion model output, *Atmos. Chem. Phys.*, 10, 669–693, doi:10.5194/acp-10-669-2010, 2010. 31830, 31841

25 Huber, P. J.: The 1972 Wald memorial lectures: robust regression: asymptotics, conjectures, and Monte Carlo, *The Annals of Statistics*, 1, 799–821, 1973. 31834

Huber, P. J.: Robust Statistics, John Wiley and Sons, Inc., New York, 1981. 31834

30 Ji, R., Jin, M., and Varpe, Ø.: Sea ice phenology and timing of primary production pulses in the Arctic Ocean, *Glob. Change Biol.*, 19, 734–741, doi:10.1111/gcb.12074, 2013. 31841

Kaufman, Y. J., Koren, I., Remer, L. A., Rosenfeld, D., and Rudich, Y.: The effect of smoke, dust, and pollution aerosol on shallow cloud development over the Atlantic Ocean, *P. Natl. Acad. Sci. USA*, 102, 11207–11212, doi:10.1073/pnas.0505191102, 2005. 31826

- Kawamoto, K., Hayasaka, T., Uno, I., and Ohara, T.: A correlative study on the relationship between modeled anthropogenic aerosol concentration and satellite-observed cloud properties over east Asia, *J. Geophys. Res.-Atmos.*, 111, 1–7, doi:10.1029/2005JD006919, 2006. 31826
- 5 Kim, B. G., Miller, M. A., Schwartz, S. E., Liu, Y., and Min, Q.: The role of adiabaticity in the aerosol first indirect effect, *J. Geophys. Res.-Atmos.*, 113, 1–13, doi:10.1029/2007JD008961, 2008. 31826
- King, M. D. and Platnick, S.: Collection 005 change summary for the MODIS cloud optical property (06 _ OD) algorithm high impact change overview: change details:, *Terra*, 1, 1–23, 10 2006. 31828
- Klein, S. A. and Hartmann, D. L.: The seasonal cycle of low stratiform clouds, *J. Climate*, 6, 1587–1606, 1993.
- 15 Klimont, Z., Smith, S. J., and Cofala, J.: The last decade of global anthropogenic sulfur dioxide: 2000–2011 emissions, *Environ. Res. Lett.*, 8, 014003, doi:10.1088/1748-9326/8/1/014003, 2013. 31840
- Klimont, Z., Hoglund, L., Heyes, C., Rafaj, P., Schoepp, W., Cofala, J., Borken-Kleefeld, J., Purohit, P., Kupiainen, K., Winiwarter, W., Amann, M., Zhao, B., Wang, S. X., Bertok, I., and Sander, R.: Global scenarios of air pollutants and methane: 1990–2050, in preparation, 2015. 31829
- 20 Lance, S., Shupe, M. D., Feingold, G., Brock, C. A., Cozic, J., Holloway, J. S., Nenes, A., Schwartz, J. P., Spackman, J. R., Froyd, K. D., Murphy, D. M., Brioude, J., Cooper, O. R., Stohl, A., and Burkhardt, J. F.: Cloud condensation nuclei as a modulator of ice processes in Arctic mixed-phase clouds, *Atmos. Chem. Phys.*, 11, 8003–8015, 2011, <http://www.atmos-chem-phys.net/11/8003/2011/>. 31825
- 25 Law, K. S. and Stohl, A.: Arctic air pollution: origins and impacts, *Science (New York, N. Y.)*, 315, 1537–40, doi:10.1126/science.1137695, 2007. 31825
- Law, K. S., Stohl, A., Quinn, P. K., Brock, C., Burkhardt, J., Paris, J. D., Ancellet, G., Singh, H. B., Roiger, A., Schlager, H., Dibb, J., Jacob, D. J., Arnold, S. R., Pelon, J., and Thomas, J. L.: 30 Arctic air pollution: new insights from POLARCAT-IPY, *B. Am. Meteorol. Soc.*, 95, 1873–1895, doi:10.1175/BAMS-D-13-00017.1, 2014. 31825
- Lihavainen, H., Kerminen, V. M., and Remer, L. A.: Aerosol-cloud interaction determined by both in situ and satellite data over a northern high-latitude site, *Atmos. Chem. Phys.*, 10, 10987–10995, doi:10.5194/acp-10-10987-2010, 2009. 31838

Title Page	
Abstract	Introduction
Conclusions	References
Tables	Figures
◀	▶
◀	▶
Back	Close
Full Screen / Esc	
Printer-friendly Version	
Interactive Discussion	



- Lindholt, L. and Glomsrød, S.: The Arctic: No big bonanza for the global petroleum industry, *Energ. Econ.*, 34, 1465–1474, doi:10.1016/j.eneco.2012.06.020, 2012. 31841
- Lohmann, U. and Feichter, J.: Global indirect aerosol effects: a review, *Atmos. Chem. Phys.*, 5, 715–737, doi:10.5194/acp-5-715-2005, 2005. 31826
- Longley, I. D., Inglis, D. W. F., Gallagher, M. W., Williams, P. I., Allan, J. D., and Coe, H.: Using NO_x and CO monitoring data to indicate fine aerosol number concentrations and emission factors in three UK conurbations, *Atmos. Environ.*, 39, 5157–5169, doi:10.1016/j.atmosenv.2005.05.017, 2005. 31826
- Lubin, D. and Vogelmann, A. M.: A climatologically significant aerosol longwave indirect effect in the Arctic, *Nature*, 439, 453–456, doi:10.1038/nature04449, 2006. 31831, 31832
- Lubin, D. and Vogelmann, A. M.: Expected magnitude of the aerosol shortwave indirect effect in springtime Arctic liquid water clouds, *Geophys. Res. Lett.*, 34, L11801, doi:10.1029/2006GL028750, 2007. 31825
- Markus, T., Stroeve, J. C., and Miller, J.: Recent changes in Arctic sea ice melt onset, freezeup, and melt season length, *J. Geophys. Res.-Oceans*, 114, 1–14, doi:10.1029/2009JC005436, 2009. 31825, 31841
- Matsui, T., Masunaga, H., Kreidenweis, S. M., Pielke, R. A., Tao, W. K., Chin, M., and Kaufman, Y. J.: Satellite-based assessment of marine low cloud variability associated with aerosol, atmospheric stability, and the diurnal cycle, *J. Geophys. Res.-Atmos.*, 111, 1–16, doi:10.1029/2005JD006097, 2006. 31831
- Mauger, G. S. and Norris, J. R.: Meteorological bias in satellite estimates of aerosol-cloud relationships, *Geophys. Res. Lett.*, 34, 1–5, doi:10.1029/2007GL029952, 2007. 31831
- Mauritsen, T., Sedlar, J., Tjernström, M., Leek, C., Martin, M., Shupe, M., Sjogren, S., Sierau, B., Persson, P. O. G., Brooks, I. M., and Swietlicki, E.: An Arctic CCN-limited cloud-aerosol regime, *Atmos. Chem. Phys.*, 11, 165–173, 2011, <http://www.atmos-chem-phys.net/11/165/2011/>. 31831, 31832
- Miller, A. W. and Ruiz, G. M.: Arctic shipping and marine invaders, *Nature Clim. Change*, 4, 413–416, doi:10.1038/nclimate2244, 2014. 31841
- Myhre, G., Stordal, F., Johnsrud, M., Kaufman, Y. J., Rosenfeld, D., Storelvmo, T., Kristjansson, J. E., Berntsen, T. K., Myhre, A., and Isaksen, I. S. A.: Aerosol-cloud interaction inferred from MODIS satellite data and global aerosol models, *Atmos. Chem. Phys.*, 7, 3081–3101, doi:10.5194/acp-7-3081-2007, 2007. 31826

Title Page	Abstract	Introduction
Conclusions	References	
Tables	Figures	
◀	▶	
◀	▶	
Back	Close	
Full Screen / Esc		
	Printer-friendly Version	
	Interactive Discussion	



Effects of pollution
on liquid clouds in
the Arctic

Q. Coopman et al.

Title Page	
Abstract	Introduction
Conclusions	References
Tables	Figures
◀	▶
◀	▶
Back	Close
Full Screen / Esc	
Printer-friendly Version	
Interactive Discussion	



- Nakajima, T., Higurashi, A., Kawamoto, K., and Penner, J. E.: A possible correlation between satellite-derived cloud and aerosol microphysical parameters, *Geophys. Res. Lett.*, 28, 1171–1174, doi:10.1029/2000GL012186, 2001. 31826
- Nygård, T., Valkonen, T., and Vihma, T.: Characteristics of arctic low-tropospheric humidity inversions based on radio soundings, *Atmos. Chem. Phys.*, 14, 1959–1971, doi:10.5194/acp-14-1959-2014, 2014. 31840
- Overland, J. E. and Wang, M.: When will the summer Arctic be nearly sea ice free?, *Geophys. Res. Lett.*, 40, 2097–2101, doi:10.1002/grl.50316, 2013. 31825
- Painemal, D., Kato, S., and Minnis, P.: Boundary layer regulation in the southeast Atlantic cloud microphysics during the biomass burning season as seen by the A-train satellite constellation, *J. Geophys. Res.-Atmos.*, 119, 11288–11302, doi:10.1002/2014JD022182, 2014. 31826
- Paris, J.-D., Stohl, A., Nédélec, P., Arshinov, M. Yu., Panchenko, M. V., Shmargunov, V. P., Law, K. S., Belan, B. D., and Ciais, P.: Wildfire smoke in the Siberian Arctic in summer: source characterization and plume evolution from airborne measurements, *Atmos. Chem. Phys.*, 9, 9315–9327, doi:10.5194/acp-9-9315-2009, 2009. 31830
- Pincus, R. and Baker, M. B.: Effect of precipitation on the albedo susceptibility of clouds in the marine boundary layer, *Nature*, 372, 250–252, doi:10.1038/372250a0, 1994. 31839
- Pizzolato, L., Howell, S. E. L., Derksen, C., Dawson, J., and Copland, L.: Changing sea ice conditions and marine transportation activity in Canadian Arctic waters between 1990 and 2012, *Climatic Change*, 123, 161–173, doi:10.1007/s10584-013-1038-3, 2014. 31841
- Platnick, S., King, M. D., Ackerman, S. A., Menzel, W. P., Baum, B. A., Riédi, J. C., and Frey, R. A.: The MODIS cloud products: Algorithms and examples from terra, *IEEE T. Geosci. Remote*, 41, 459–472, doi:10.1109/TGRS.2002.808301, 2003. 31828
- Qiu, S., Dong, X., Xi, B., and Li, J. F.: Characterizing Arctic mixed-phase cloud structure and its relationship with humidity and temperature inversion using ARM NSA observations, *J. Geophys. Res.*, 120, 7737–7746, doi:10.1002/2014JD023022.Received, 2015. 31840
- Quinn, P. K., Shaw, G., Andrews, E., Dutton, E. G., Ruoho-Airola, T., and Gong, S. L.: Arctic haze: Current trends and knowledge gaps, *Tellus B*, 59, 99–114, doi:10.1111/j.1600-0889.2006.00238.x, 2007. 31825
- Richter-Menge, J. and Jeffries, M.: State of the climate in 2010: The Arctic, *B. Am. Meteorol. Soc.*, 92, S143–S160, 2011. 31825

- Riedi, J., Marchant, B., Platnick, S., Baum, B. A., Thieuleux, F., Oudard, C., Parol, F., Nicolas, J.-M., and Dubuisson, P.: Cloud thermodynamic phase inferred from merged POLDER and MODIS data, *Atmos. Chem. Phys.*, 10, 11851–11865, 2010,
<http://www.atmos-chem-phys.net/10/11851/2010/>. 31829
- 5 Schwartz, S. E., Harshvardhan, and Benkovitz, C. M.: Influence of anthropogenic aerosol on cloud optical depth and albedo shown by satellite measurements and chemical transport modeling, *P. Natl. Acad. Sci. USA*, 99, 1784–1789, doi:10.1073/pnas.261712099, 2002.
 31826
- 10 Sekiguchi, M.: A study of the direct and indirect effects of aerosols using global satellite data sets of aerosol and cloud parameters, *J. Geophys. Res.*, 108, 1–15, doi:10.1029/2002JD003359, 2003. 31826
- Serreze, M. C. and Francis, J. A.: The Arctic on the fast track of change, *Weather*, 61, 65–69, doi:10.1256/wea.197.05, 2006. 31825
- 15 Serreze, M. C., Barrett, A. P., Stroeve, J. C., Kindig, D. N., and Holland, M. M.: The emergence of surface-based Arctic amplification, *The Cryosphere*, 3, 11–19, doi:10.5194/tc-3-11-2009, 2009. 31825
- Shaw, G. E.: The arctic haze phenomenon, *B. Am. Meteorol. Soc.*, 76, 2403–2413, doi:10.1175/1520-0477(1995)076<2403:TAHP>2.0.CO;2, 1995. 31825
- 20 Shindell, D. T., Chin, M., Dentener, F., Doherty, R. M., Faluvegi, G., Fiore, A. M., Hess, P., Koch, D. M., MacKenzie, I. A., Sanderson, M. G., Schultz, M. G., Schulz, M., Stevenson, D. S., Teich, H., Textor, C., Wild, O., Bergmann, D. J., Bey, I., Bian, H., Cuvelier, C., Duncan, B. N., Folberth, G., Horowitz, L. W., Jonson, J., Kaminski, J. W., Marmer, E., Park, R., Pringle, K. J., Schroeder, S., Szopa, S., Takemura, T., Zeng, G., Keating, T. J., and Zuber, A.: A multi-model assessment of pollution transport to the Arctic, *Atmos. Chem. Phys.*, 8, 5353–5372, 2008,
<http://www.atmos-chem-phys.net/8/5353/2008/>. 31825
- 25 Sirois, A. and Barrie, L. A.: Arctic lower tropospheric aerosol trends and composition at Alert, Canada: 1980–1995, *J. Geophys. Res.*, 104, 11599, doi:10.1029/1999JD900077, 1999. 31825
- 30 Sodemann, H., Pommier, M., Arnold, S. R., Monks, S. A., Stebel, K., Burkhardt, J. F., Hair, J. W., Diskin, G. S., Clerbaux, C., Coheur, P.-F., Hurtmans, D., Schlager, H., Blechschmidt, A.-M., Kristjánsson, J. E., and Stohl, A.: Episodes of cross-polar transport in the Arctic troposphere during July 2008 as seen from models, satellite, and aircraft observations, *Atmos. Chem.*

[Title Page](#)[Abstract](#)[Introduction](#)[Conclusions](#)[References](#)[Tables](#)[Figures](#)[|◀](#)[▶|](#)[◀](#)[▶](#)[Back](#)[Close](#)[Full Screen / Esc](#)[Printer-friendly Version](#)[Interactive Discussion](#)

5 Sporre, M. K., Glantz, P., Tunved, P., Swietlicki, E., Kulmala, M., and Lihavainen, H.: A study of the indirect aerosol effect on subarctic marine liquid low-level clouds using MODIS cloud data and ground-based aerosol measurements, *Atmos. Res.*, 116, 56–66, doi:10.1016/j.atmosres.2011.09.014, 2012. 31838

10 Stephens, G. L., Vane, D. G., Boain, R. J., Mace, G. G., Sassen, K., Wang, Z., Illingworth, A. J., O'Connor, E. J., Rossow, W. B., Durden, S. L., Miller, S. D., Austin, R. T., Benedetti, A., and Mitrescu, C.: The cloudsat mission and the A-Train: A new dimension of space-based observations of clouds and precipitation, *B. Am. Meteorol. Soc.*, 83, 1771–1790+1742, doi:10.1175/BAMS-83-12-1771, 2002. 31828

Stohl, A.: Characteristics of atmospheric transport into the Arctic troposphere, *J. Geophys. Res.*, 111, D11306, doi:10.1029/2005JD006888, 2006. 31825, 31827, 31830, 31839

15 Stohl, A., Hitzenberger, M., and Wotawa, G.: Validation of the lagrangian particle dispersion model FLEXPART against large-scale tracer experiment data, *Atmos. Environ.*, 32, 4245–4264, doi:10.1016/S1352-2310(98)00184-8, 1998. 31829

Stohl, A., Franck, A., Seibert, P., and Wotawa, G.: Technical note: The lagrangian particle dispersion model FLEXPART version 6.2, *Atmos. Chem. Phys.*, 5, 2005. 31827, 31829

20 Stohl, A., Berg, T., Burkhardt, J. F., Fjæraa, A. M., Forster, C., Herber, A., Hov, Ø., Lunder, C., McMillan, W. W., Oltmans, S., Shiobara, M., Simpson, D., Solberg, S., Stebel, K., Ström, J., Tørseth, K., Treffisen, R., Virkkunen, K., and Yttri, K. E.: Arctic smoke – record high air pollution levels in the European Arctic due to agricultural fires in Eastern Europe in spring 2006, *Atmos. Chem. Phys.*, 7, 511–534, doi:10.5194/acp-7-511-2007, 2007. 31825

25 Stohl, A., Klimont, Z., Eckhardt, S., Kupiainen, K., Shevchenko, V. P., Kopeikin, V. M., and Novigatsky, A. N.: Black carbon in the Arctic: the underestimated role of gas flaring and residential combustion emissions, *Atmos. Chem. Phys.*, 13, 8833–8855, doi:10.5194/acp-13-8833-2013, 2013. 31829, 31830

30 Stohl, A., Aamaas, B., Amann, M., Baker, L. H., Bellouin, N., Berntsen, T. K., Boucher, O., Cherian, R., Collins, W., Daskalakis, N., Dusinska, M., Eckhardt, S., Fuglestvedt, J. S., Harju, M., Heyes, C., Hodnebrog, Ø., Hao, J., Im, U., Kanakidou, M., Klimont, Z., Kupiainen, K., Law, K. S., Lund, M. T., Maas, R., MacIntosh, C. R., Myhre, G., Myriokefalitakis, S., Olivié, D., Quaas, J., Quennehen, B., Raut, J.-C., Rumbold, S. T., Samset, B. H., Schulz, M., Seland, Ø., Shine, K. P., Skeie, R. B., Wang, S., Yttri, K. E., and Zhu, T.: Evaluating the climate

Effects of pollution
on liquid clouds in
the Arctic

Q. Coopman et al.

Title Page	
Abstract	Introduction
Conclusions	References
Tables	Figures
◀	▶
◀	▶
Back	Close
Full Screen / Esc	
Printer-friendly Version	
Interactive Discussion	



and air quality impacts of short-lived pollutants, *Atmos. Chem. Phys.*, 15, 10529–10566, doi:10.5194/acp-15-10529-2015, 2015. 31829, 31830

Tietze, K., Riedi, J., Stohl, A., and Garrett, T. J.: Space-based evaluation of interactions between aerosols and low-level Arctic clouds during the Spring and Summer of 2008, *Atmos. Chem. Phys.*, 11, 3359–3373, 2011,
5 <http://www.atmos-chem-phys.net/11/3359/2011/>. 31827, 31828, 31833, 31838, 31839

Venables, W. N. and Ripley, B. D.: *Modern Applied Statistics with S-PLUS*, Springer Science and Business Media, New York, NY, 2013. 31834

Wang, F., Guo, J., Wu, Y., Zhang, X., Deng, M., Li, X., Zhang, J., and Zhao, J.: Satellite observed aerosol-induced variability in warm cloud properties under different meteorological conditions over eastern China, *Atmos. Environ.*, 84, 122–132, doi:10.1016/j.atmosenv.2013.11.018,
10 2014. 31826

Warneke, C., Bahreini, R., Brioude, J., Brock, C. A., De Gouw, J. A., Fahey, D. W., Froyd, K. D., Holloway, J. S., Middlebrook, A., Miller, L., Montzka, S., Murphy, D. M., Peischl, J., Ryerson, T. B., Schwarz, J. P., Spademan, J. R., and Veres, P.: Biomass burning in Siberia and Kazakhstan as an important source for haze over the Alaskan Arctic in April 2008, *Geophys. Res. Lett.*, 36, 2–7, doi:10.1029/2008GL036194, 2009. 31830

Weisz, E., Li, J., Menzel, W. P., Heidinger, A. K., Kahn, B. H., and Liu, C. Y.: Comparison of AIRS, MODIS, CloudSat and CALIPSO cloud top height retrievals, *Geophys. Res. Lett.*, 34, 20 1–5, doi:10.1029/2007GL030676, 2007. 31828

Wesslén, C., Tjernström, M., Bromwich, D. H., De Boer, G., Ekman, A. M. L., Bai, L. S., and Wang, S. H.: The Arctic summer atmosphere: An evaluation of reanalyses using ASCOS data, *Atmos. Chem. Phys.*, 14, 2605–2624, doi:10.5194/acp-14-2605-2014, 2014. 31830

Westerling, A. L., Hidalgo, H. G., Cayan, D. R., and Swetnam, T. W.: Warming and earlier spring increase western U. S. forest wildfire activity, *Science (New York, N. Y.)*, 313, 940–943, doi:10.1126/science.1128834, 2006. 31841

Yoshimori, M., Watanabe, M., Abe-Ouchi, A., Shiogama, H., and Ogura, T.: Relative contribution of feedback processes to Arctic amplification of temperature change in MIROC GCM, *Clim. Dynam.*, 42, 1613–1630, doi:10.1007/s00382-013-1875-9, 2013. 31825

Zhao, C. and Garrett, T. J.: Effects of Arctic Haze on surface Cloud radiative forcing, *Geophys. Res. Lett.*, 42, 557–564, doi:10.1002/2014GL062015, 2015. 31825

Effects of pollution
on liquid clouds in
the Arctic

Q. Coopman et al.

Title Page

Abstract

Introduction

Conclusions

References

Tables

Figures

◀

▶

◀

▶

Back

Close

Full Screen / Esc

Printer-friendly Version

Interactive Discussion



Zhao, C., Klein, S. A., Xie, S., Liu, X., Boyle, J. S., and Zhang, Y.: Aerosol first indirect effects on non-precipitating low-level liquid cloud properties as simulated by CAM5 at ARM sites, Geophys. Res. Lett., 39, 1–7, doi:10.1029/2012GL051213, 2012. 31838

5 Zygmuntowska, M., Mauritzen, T., Quaas, J., and Kaleschke, L.: Arctic clouds and surface radiation—a critical comparison of satellite retrievals and the ERA-interim reanalysis, Atmos. Chem. Phys., 12, 6667–6677, doi:10.5194/acp-12-6667-2012, 2012. 31830

Effects of pollution on liquid clouds in the Arctic

Q. Coopman et al.

[Title Page](#)

[Abstract](#)

[Introduction](#)

[Conclusions](#)

[References](#)

[Tables](#)

[Figures](#)



[◀](#)

[▶](#)

[Back](#)

[Close](#)

[Full Screen / Esc](#)

[Printer-friendly Version](#)

[Interactive Discussion](#)



**Effects of pollution
on liquid clouds in
the Arctic**

Q. Coopman et al.

Table 1. Cloud products, pollution tracer, atmospheric reanalysis used in this study with the corresponding spatial and temporal resolution.

Parameter(s)	From:	Resolution(s)
Cloud parameter (T , r_e , τ)	MODIS, POLDER-3	Spatial resolution: 36 km^2
CO tracer concentration from anthropogenic sources	FLEXPART	Spatial resolution: $1^\circ \times 2^\circ$, Temporal resolution: 3 h
Specific humidity, temperature profile	ERA-I (ECMWF)	Spatial resolution: $1.5^\circ \times 1.5^\circ$, Temporal resolution: 6 h

Effects of pollution on liquid clouds in the Arctic

Q. Coopman et al.

Table 2. Summary of the different ranges of the logarithm of the specific humidity and the LTS over the region of interest, detailing the method used to determine the final range of parameters considered. The Δ defines the difference between the maximum and the minimum of the total range. The considered range is chosen to keep the maximum number of measurements within a fixed interval of 15 % of the range, corresponding to the red square on Fig. 4.

	\log_{10} (Specific Humidity)	LTS (°)
Total Range [Min, Max]	[−0.89, 1.0]	[2.1, 38]
Δ Total Range	1.9	36
15 % Interval	0.28	5.4
Constrained Range [Min, Max]	[0.30, 0.60] = [2.0, 4.0] (g kg^{-1})	[17, 22]

[Title Page](#)

[Abstract](#)

[Introduction](#)

[Conclusions](#)

[References](#)

[Tables](#)

[Figures](#)

◀

▶

◀

▶

[Back](#)

[Close](#)

[Full Screen / Esc](#)

[Printer-friendly Version](#)

[Interactive Discussion](#)



**Effects of pollution
on liquid clouds in
the Arctic**

Q. Coopman et al.

Table 3. IE parameter calculated for the optical depth and the effective radius considering all clouds, graybody clouds and blackbody clouds, averaged from values presented in Fig. 5 and weighted considering the inverse of the uncertainty in the mean.

	All LWP	Graybody	Blackbody
IE_{r_e}	0.12	0.10	0.14
IE_τ	0.16	0.13	0.17

Effects of pollution on liquid clouds in the Arctic

Q. Coopman et al.

Table 4. IE parameter calculated for the optical depth and the effective radius considering all clouds, graybody clouds, and blackbody clouds, for two different regimes of CO concentration representing lower and upper quartiles of CO concentration.

	All LWP		Graybody		Blackbody	
	IE_{r_e}	IE_τ	IE_{r_e}	IE_τ	IE_{r_e}	IE_τ
$\chi_{\text{CO}} < 5.5 \text{ ppbv}$	0.23	0.36	0.31	0.26	0.28	0.24
$\chi_{\text{CO}} > 10 \text{ ppbv}$	0.09	0.35	0.09	0.16	0.14	0.16

- [Title Page](#)
- [Abstract](#) | [Introduction](#)
- [Conclusions](#) | [References](#)
- [Tables](#) | [Figures](#)
- [◀](#) | [▶](#)
- [◀](#) | [▶](#)
- [Back](#) | [Close](#)
- [Full Screen / Esc](#)
- [Printer-friendly Version](#)
- [Interactive Discussion](#)



**Effects of pollution
on liquid clouds in
the Arctic**

Q. Coopman et al.

Table 5. Percentile values of specific humidity and LTS used to defined different regimes of the meteorological parameters.

	Specific Humidity (g kg^{-1})	LTS (K)
Minimum	0.13	2.1
20th percentile	1.2	14
40th percentile	1.7	18
60th percentile	2.4	20
80th percentile	3.6	23
Maximum	11	37

**Effects of pollution
on liquid clouds in
the Arctic**

Q. Coopman et al.

Table 6. Difference between IE_{τ} and IE_{r_e} (i.e. IE_{LWP}) for graybody, blackbody, and all clouds when the data are constrained for lower tropospheric stability and specific humidity and when they are not constrained. The averaged IE values are shown in Table 3.

	All LWP	Graybody	Blackbody
Constrained	0.04	0.03	0.04
Not constrained	0.12	0.04	0.08

**Effects of pollution
on liquid clouds in
the Arctic**

Q. Coopman et al.

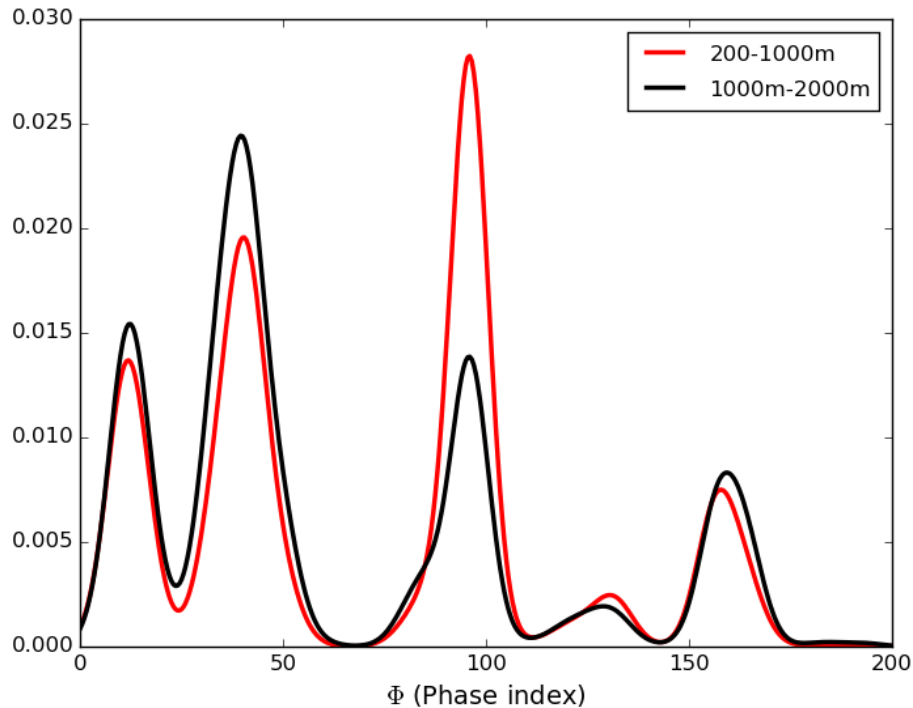


Figure 1. Normalized cloud thermodynamic phase index frequency distribution from the POLDER-MODIS algorithm, for pixels with the phase-index SD less than 10. Colors represent different cloud altitudes, between 200–1000 m in red and between 1000–2000 m in black.

**Effects of pollution
on liquid clouds in
the Arctic**

Q. Coopman et al.

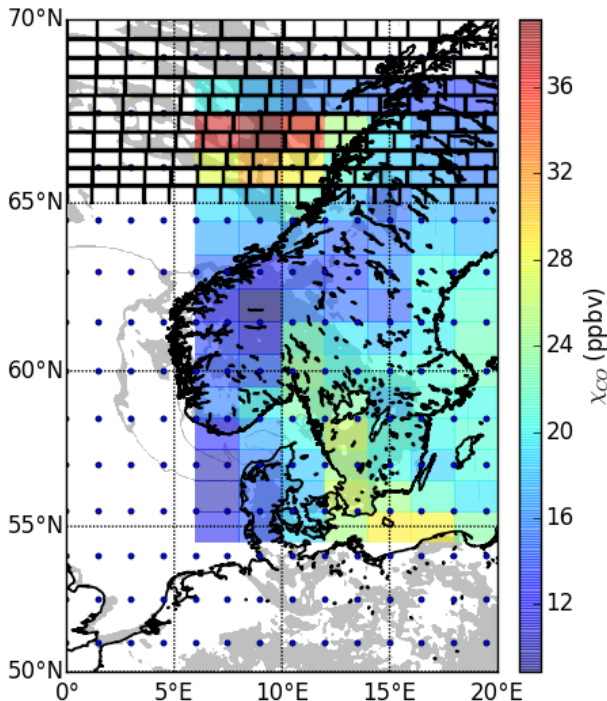


Figure 2. Illustration of the horizontal co-location method, showing satellite data corresponding to cloud top pressures below 1000 m altitude (gray shading), the average FLEXPART CO concentration between 1 and 2 km (colored shading), and the spatial resolution of temperature profiles and specific humidity in blue points. The black grid, on the top of the map, corresponds to the sinusoidal equal-area grid used in this study for co-locating each data set.

Title Page	Abstract	Introduction
Conclusions	References	
Tables	Figures	
◀	▶	
◀	▶	
Back	Close	
Full Screen / Esc		
	Printer-friendly Version	
	Interactive Discussion	



**Effects of pollution
on liquid clouds in
the Arctic**

Q. Coopman et al.

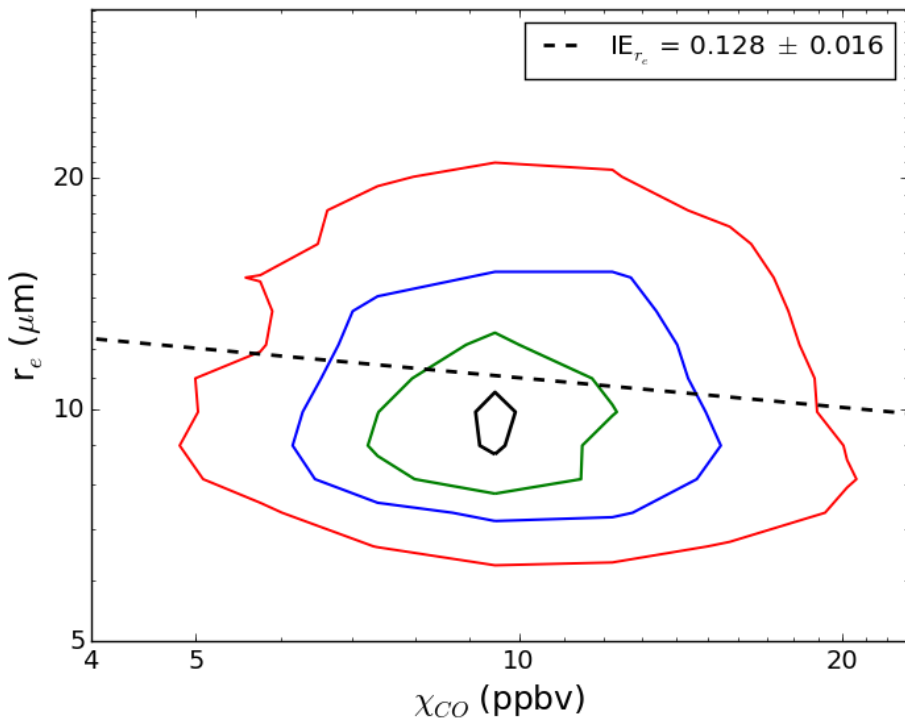


Figure 3. Calculation of the IE parameter from a probability distribution of values in the effective radius and CO tracer concentration for liquid clouds with cloud top altitudes below 2000 m, and cloud top temperatures between -12 and 6.0°C . The color scale indicates higher density of values in linear intervals. The IE number indicates the negative slope of the linear fit (dashed line).

**Effects of pollution
on liquid clouds in
the Arctic**

Q. Coopman et al.

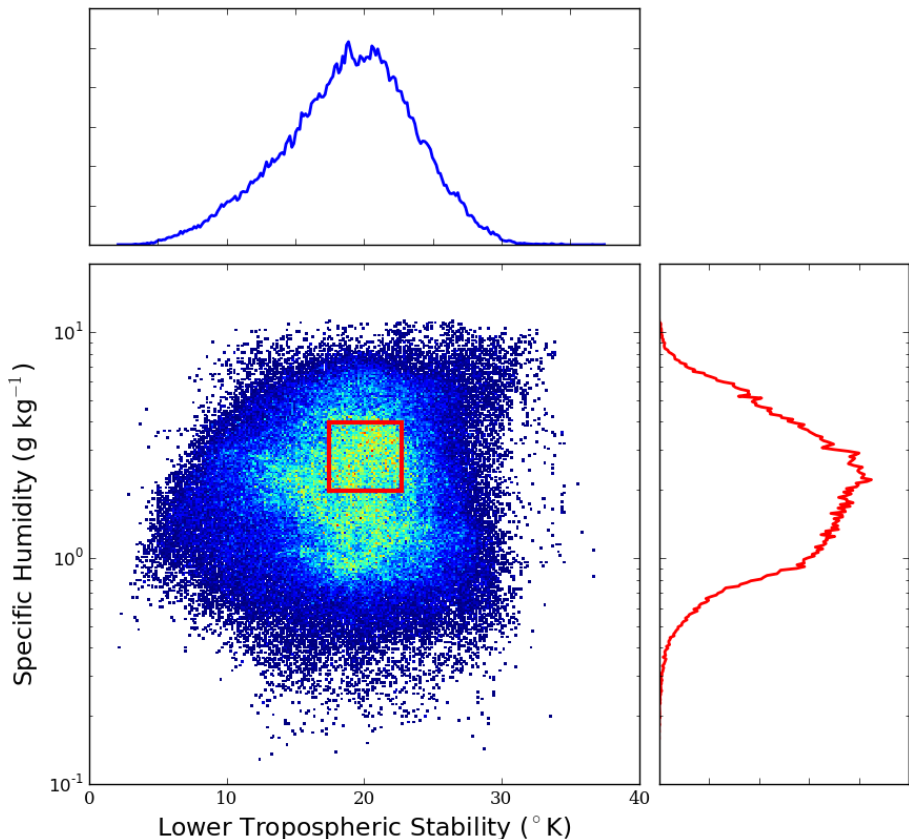


Figure 4. 2-D histogram of the specific humidity and the LTS retrieved by ECMWF reanalysis from 2008 to 2010. The red rectangle corresponds to the range where there is a maximum of measurements within a bin corresponding to 15 % of the total range length of the corresponding parameter.

Title Page	Abstract	Introduction
Conclusions	References	
Tables	Figures	
◀	▶	
◀	▶	
Back	Close	
Full Screen / Esc		
Printer-friendly Version		
Interactive Discussion		



Effects of pollution on liquid clouds in the Arctic

Q. Coopman et al.

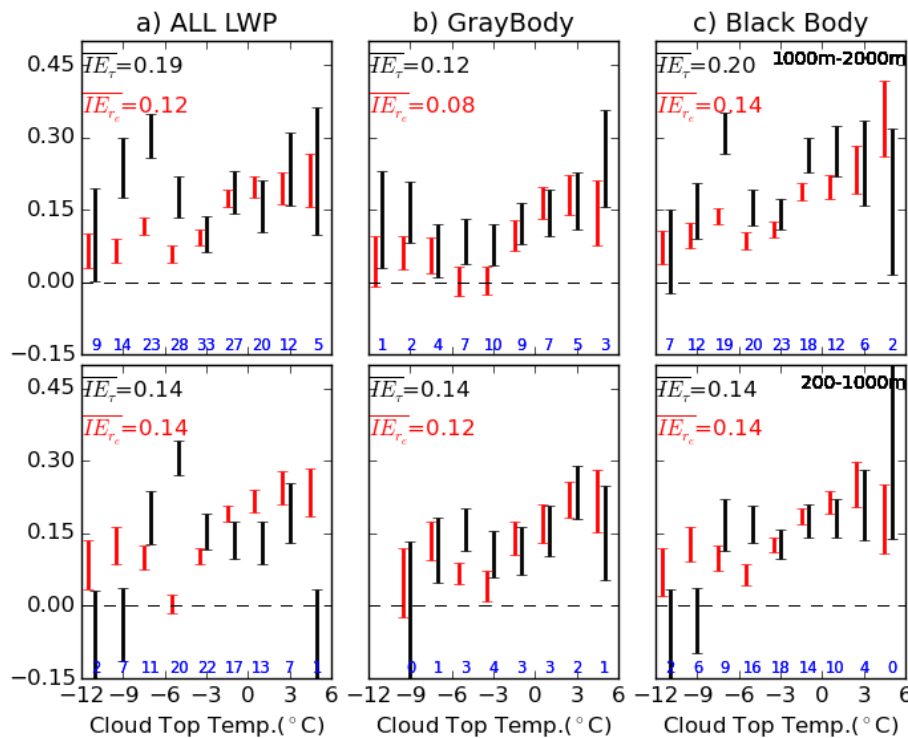


Figure 5. IE parameter of the effective radius (r_e) (red) and optical depth (τ) (black), as a function of temperature calculated for liquid clouds between 200–1000 m (lower row) and 1000–2000 m (upper row). The bars indicate the 95 % confidence limit in the calculation of the mean IE value. Each column corresponds to different thresholds for LWP (blackbody: $\text{LWP} > 40 \text{ g m}^{-2}$, graybody: $\text{LWP} < 40 \text{ g m}^{-2}$). Blue numbers indicate the number of grid-cells, in hundreds, that are used to calculate each IE value. In each figure the IE value averaged over the temperature and weighted according the inverse of the uncertainty is indicated.

**Effects of pollution
on liquid clouds in
the Arctic**

Q. Coopman et al.

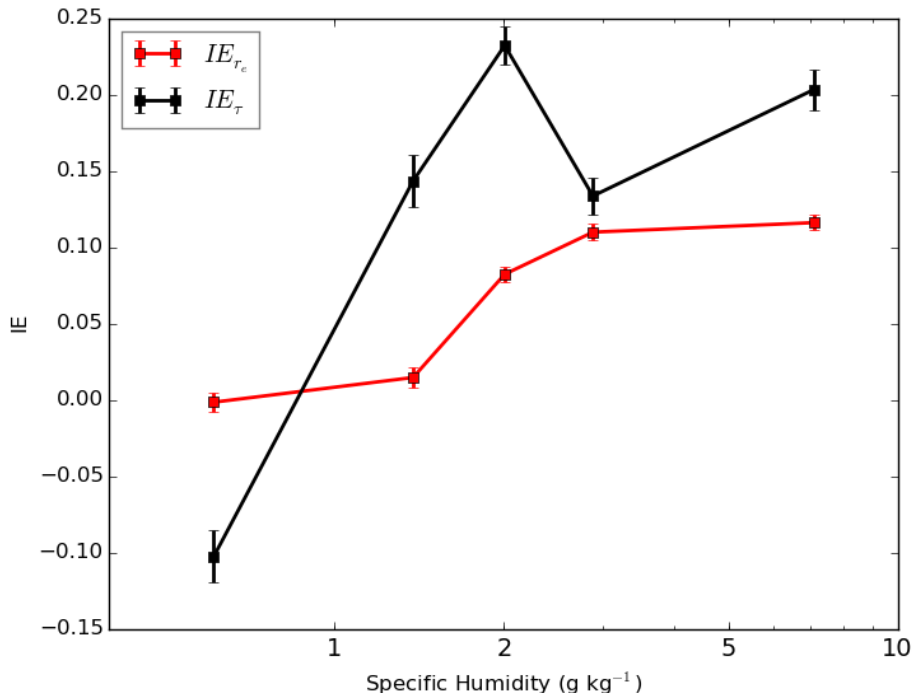


Figure 6. IE_{r_e} (red) and IE_τ (black) for different bins of the specific humidity, constrained for values of LTS between 17 and 22 K. Each marker is placed in the middle of the corresponding bin.

**Effects of pollution
on liquid clouds in
the Arctic**

Q. Coopman et al.

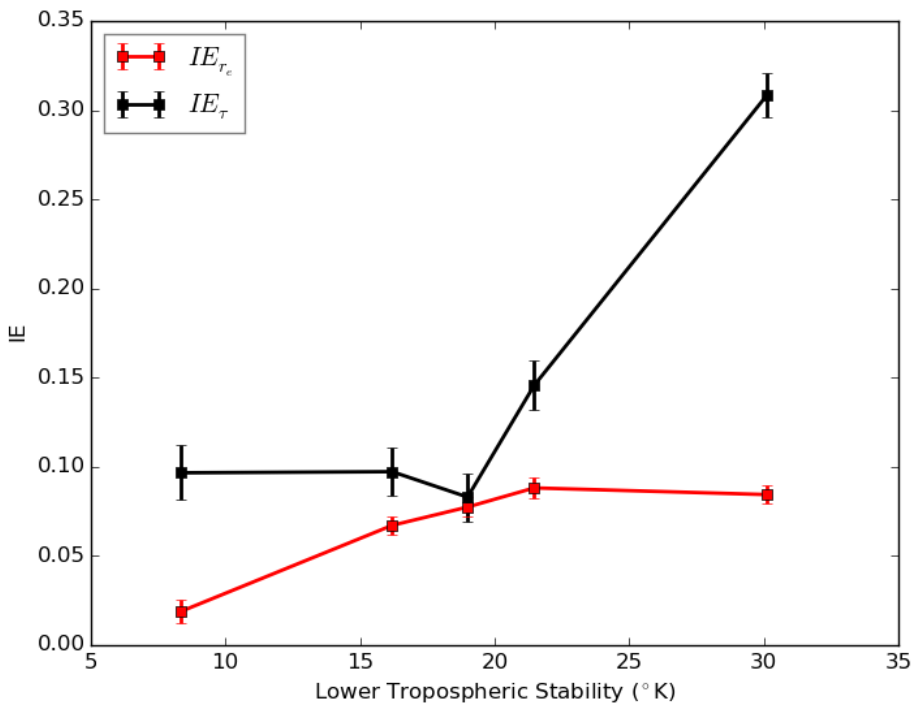


Figure 7. IE_{r_e} (red) and IE_{τ} (black) and IE_{τ} as a function of the lower tropospheric stability, constrained for values of specific humidity between 2.0 and 4.0 g kg^{-1} .

**Effects of pollution
on liquid clouds in
the Arctic**

Q. Coopman et al.

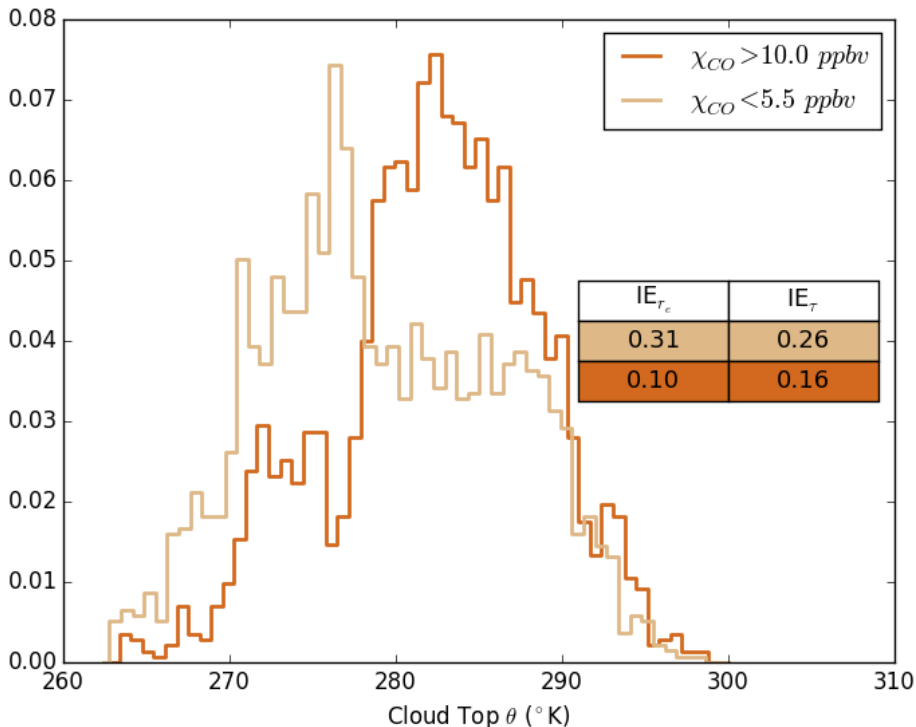


Figure 8. Normalized distribution of the cloud top potential temperature when clouds are associated with CO tracer concentrations (χ_{CO}) greater than 10 ppbv and less than 5 ppbv. The values of IE_{r_e} and IE_τ associated with each histogram are presented also in Table 3.